Structural constraints in neotectonic studies of thrust faults from the magnetotelluric method, Kochkor Basin, Kyrgyz Republic

Stephen K. Park,[1] Stephen C. Thompson,[2,3] Anatoly Rybin,[4] Vladimir Batalev,[4] and Robert Bielinski[1]

Received 13 July 2001; revised 18 September 2002; accepted 5 February 2003; published 15 April 2003.

[1] A continuous high-resolution magnetotelluric (MT) profile 5.4 km long reveals a 1- to 2-km-thick section of Neogene strata thrust beneath a crystalline range front along a gently dipping décollement in the Kyrgyz Tien Shan, central Asia. The imaged décollement links the intrabasin Akchop Hills fault, which currently accommodates ~15% of the total shortening across the central Tien Shan, to a crustal ramp that dips ~45° beneath the range. Bounds from the MT data on the base of the sediments and on the dip of the crustal ramp suggest >2.5–7.5 km of total shortening across the basin margin, of which at least 2.5–4.8 km clearly involves the décollement and the recently developed Akchop Hills fault. Thus a significant fraction of the total shortening across the margin has been accommodated by this young fault system. Combined with preliminary studies that suggest a mid-Miocene age for the base of the stratigraphic section, results drawn from the MT section indicate that shortening rates have increased since the onset of deformation, perhaps within the past 1–2 million years. *INDEX TERMS:* 8107 Tectonophysics: Continental neotectonics; 8102 Tectonophysics: Continental contractional orogenic belts; 8010 Structural Geology: Fractures and faults; 0925 Exploration Geophysics: Magnetic and electrical methods; *KEYWORDS:* Asia tectonics, magnetotelluric method, Tien Shan, Kyrgyzstan. **Citation:** Park, S. K., S. C. Thompson, A. Rybin, V. Batalev, and R. Bielinski, Structural constraints in neotectonic studies of thrust faults from the magnetotelluric method, Kochkor Basin, Kyrgyz Republic, *Tectonics*, *22*(2), 1013, doi:10.1029/2001TC001318, 2003.

1. Introduction

[2] Thick-skinned mountain building, although prevalent in the deformation of Earth's continents, has been difficult to characterize owing to heterogeneities in basement rocks involved in deformation [*Rodgers and Rizer*, 1981]. Moderately and gently dipping thrust faults that underlie many thick-skinned ranges [*Berg*, 1962; *Smithson et al.*, 1978; *Gries*, 1983; *Snyder et al.*, 1990; *Beauchamp et al.*, 1999] extend to the surface as moderate- to high-angle reverse faults and/or abrupt folds that separate crystalline ranges from adjacent basins [*Jordan and Allmendinger*, 1986; *Schmidt et al.*, 1993]. While many thick-skinned mountains show deformation localized near the range front, there are several examples of basement-involved ranges where deformation extends several to tens of kilometers into the adjacent foreland basin. Commonly, the intrabasin thrust faults are interpreted to connect with crustal ramps that underlie the ranges along a décollement. This fault geometry requires anticlinal folding of basement rocks in the hanging wall as material moves over the fault bend [*Narr and Suppe*, 1994] and underthrusting of sediments beneath the range front if the level of décollement is above the base of basin strata. Modern examples show faults and folds within the basins to be more active than structures that bound the basement range front [*Ikeda*, 1983; *Avouac et al.*, 1993; *Benedetti et al.*, 2000; *Thompson et al.*, 2002].

[3] Active faults within late Cenozoic basins permeate the Tien Shan of central Asia (Figure 1). Late Cenozoic activity in the Tien Shan results from India-Eurasia collision and produces crustal shortening and thickening by thrust faulting and folding of crystalline to low-grade metamorphic basement blocks against intervening synorogenic basins [*Tapponnier and Molnar*, 1979]. Across the central portion of the belt, within Kyrgyzstan, nearly every intermontane basin contains active faults and fault-related folds that lie several to tens of kilometers from deformed range-basin margins [*Sadybakasov*, 1972; *Makarov*, 1977]. Geologic mapping and river terrace profiles here and elsewhere in the Tien Shan indicate that thrust faults in the basins bend to décollements within synorogenic strata that dip gently toward the mountain fronts [*Avouac et al.*, 1993; *Burchfiel et al.*, 1999; *Abdrakhmatov et al.*, 2001]. The highest late Quaternary slip rates across the central Tien Shan occur on these faults, indicating that recent shortening is accommodated preferentially at the surface on these intrabasin thrusts rather than on faults that delineate the range front [*Thompson et al.*, 2002]. Although the décollements are inferred to connect to more steeply dipping crustal ramps beneath the range front, the subsurface geometry of the active basin margin and dip of the crustal ramp lack constraints by geophysical data.

[4] A high-resolution magnetotelluric (MT) profile was conducted across the southern margin of the Kochkor basin

[1]Institute of Geophysics and Planetary Physics, University of California, Riverside, California, USA.
[2]Department of Earth and Space Sciences, University of Washington, Seattle, Washington, USA.
[3]Now at Department of Geological Sciences, University of Oregon, Eugene, Oregon, USA.
[4]Institute for High Temperatures of the Russian Academy of Sciences Scientific Station, Bishkek, Kyrgyz Republic.

0278-7407/03/2001TC001318

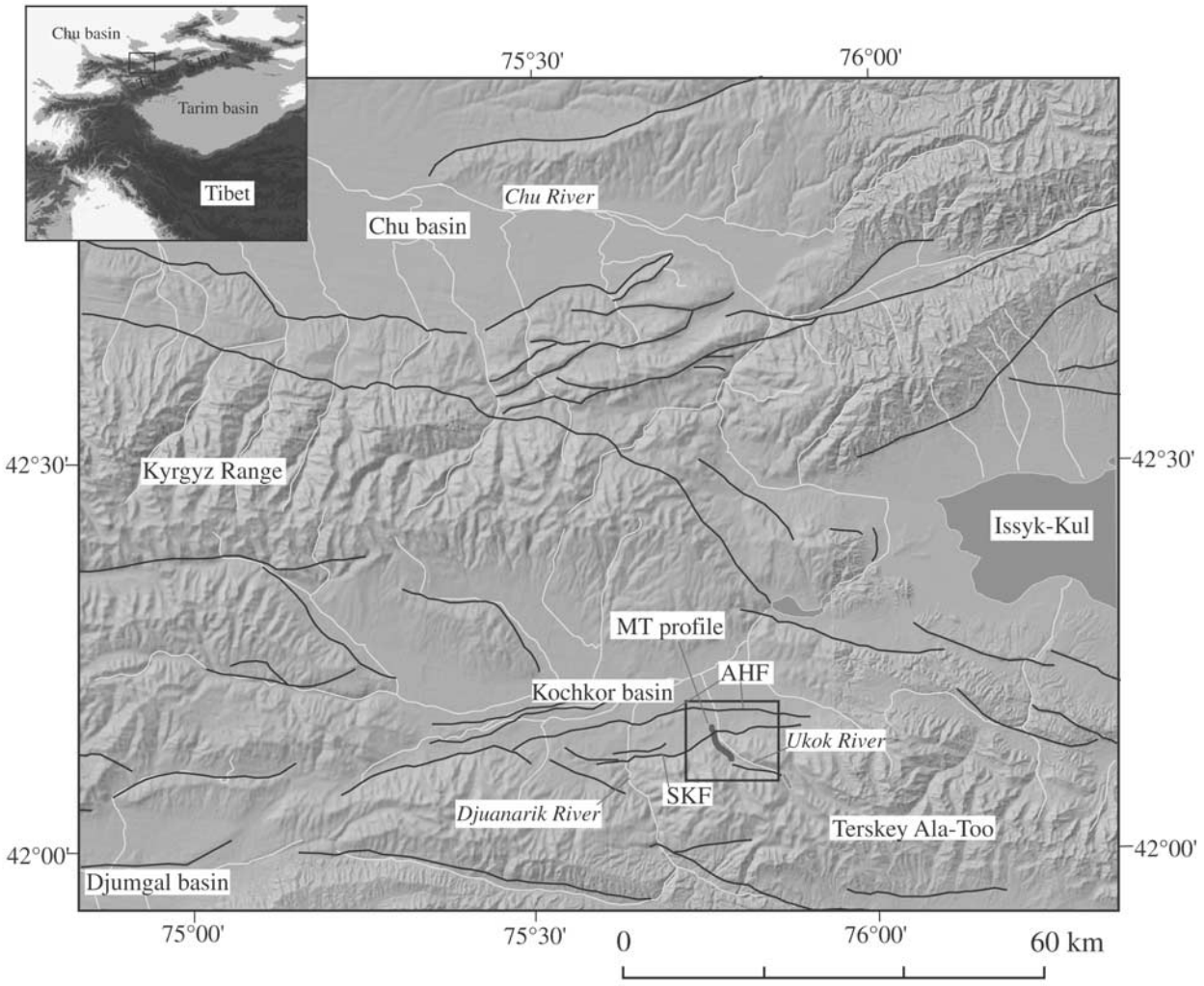

Figure 1. Shaded relief map of the Kochkor basin and surrounding ranges and basins in the Kyrgyz Tien Shan. Solid lines show late Cenozoic faults; white lines indicate rivers. The location of the magnetotelluric (MT) profile along the Ukok River is indicated by the bold line and lies within the solid box (Figure 2). The inset shows the location of the Tien Shan in central Asia. The topographic base is from a 1-km digital elevation model [*Global Land One-Kilometer Base Elevation Task Team et al.*, 1999]. AHF is Akchop Hills fault; SKF is South Kochkor fault.

(Figure 1) in order to map the orientation and location of the crustal ramp and the depth and lateral extent of subthrust sediments. Limits on these parameters serve two purposes: First, constraints on the subsurface fault geometry will help correlate late Quaternary slip rates, measured on faults within the basins, to crustal shortening through the upper-middle crust, thereby providing a means to better compare geologic and geodetic shortening rates [*Meade and Hager*, 2001; *Thompson et al.*, 2002]. Second, subsurface constraints will allow us to place limits on total late Cenozoic shortening across this range-basin margin and permit us to evaluate the style and partitioning of late Cenozoic shortening between structures that bound the basin margins and faults that penetrate the syntectonic basins.

[5] The MT method is utilized to map the distribution of conductive rocks in the Earth. Enhanced conductivity can be caused by partial melt, conductive minerals, and/or aqueous fluids and requires that the conductive component(s) in the rock be interconnected. In this study of a shallow sedimentary section the increased conductivity of the sediments over that of the basement rocks will be due to the higher porosities in those sediments. Use of the MT method to map sediments in the footwall of a thrust fault is not new [e.g., *Bedrosian et al.*, 2001], and high-resolution studies have imaged details of strike-slip fault zones [*Unsworth et al.*, 1997]. However,

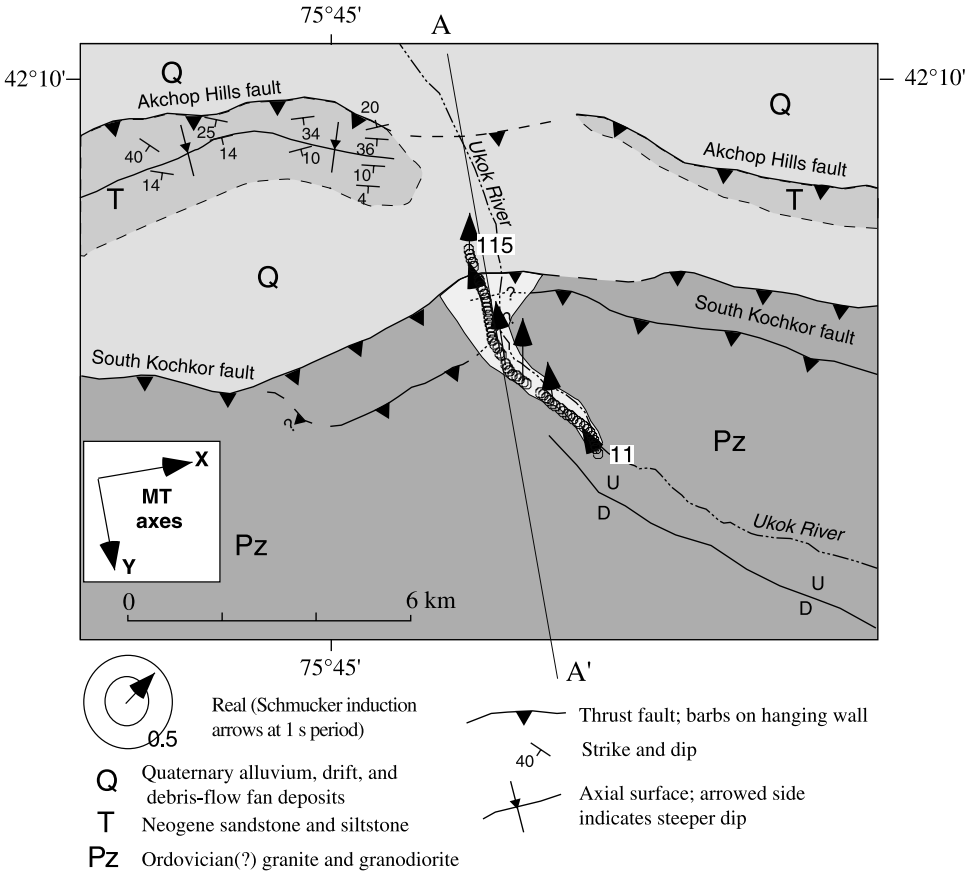

Figure 2. Geologic map of the Ukok River region showing thrust faults and the location of the MT profile (circles). The map is based on aerial photograph interpretation and limited surface observations. Beginning and ending MT site numbers are given, and orientations of the MT principal axes are shown with the inset. Also plotted are the real components of the Schmucker induction arrows for a period of 1 s at several MT stations along the profile; these arrows point toward conductors by convention and are responding to the sediments in the Kochkor basin to the north and west (Figure 1). The north-south cross-section line corresponds to Figure 6.

this is the first high-resolution profile coupled specifically with a neotectonic study of a thrust fault.

2. Kochkor Basin

[6] The Kochkor basin, surrounded to the north and south by the >4000-m-high peaks of the Kyrgyz Range and the Terskey Ala-Too, lies 40 km south of the Chu basin and the northern front of the central Tien Shan (Figure 1). The late Quaternary shortening rate of $\sim$3 mm yr^{-1} across the southern margin of the basin, measured near the Djuanarik River, represents $\sim$15% of the current shortening across the central Tien Shan [*Thompson et al.*, 2002]. The South Kochkor fault places polyphase-deformed Paleozoic granitic and metasedimentary rock of the Terskey Ala-Too over Neogene and Quaternary sediments of the Kochkor basin (Figure 2). The depth of the basin is estimated to be $\sim$2–4 km at its southern margin, and sediments taper to zero at the northern margin where they overlap a Paleozoic-early Cenozoic unconformity [*Abdrakhmatov et al.*, 2001].

[7] Faulted and folded Neogene strata and late Quaternary river terraces show that most Quaternary shortening in the central Kochkor basin has occurred on the Akchop Hills fault, which lies $\sim$4–8 km north of the range front (Figure 2). Although the fault is not exposed, mapping within the hanging wall suggests that the Akchop Hills fault dips 30°–45°S at the surface and shallows to a dip of <10° parallel to bedding. This gently south dipping décollement is inferred to intersect the South Kochkor fault at a depth of less than a few kilometers beneath the Terskey Ala-Too range front. Low-lying river terraces along the Djuanarik River extend 2 km into the range and suggest that the décollement continues to at least that far south of the range front before it presumably intersects a more steeply dipping ramp that underlies the range [*Thompson et al.*, 2002]. Independent evidence of the inferred fault geometry and the extent of underthrusting of sediment beneath the margin will allow a better constraint on the style and total amount of shortening across this intermontane basin margin, which serves as a prototype for other active intermontane basin margins across

the central Tien Shan. While the dip of the crustal-scale ramp is unknown, intermediate dips are likely based on focal mechanisms of moderate-sized earthquakes [*Ghose et al.*, 1998] and the $Ms = 7.3$ Suusamyr earthquake, which occurred on a south dipping ramp with a dip of $\sim 50^\circ$ in a similar tectonic setting $\sim$100 km to the west [*Mellors et al.*, 1997].

3. Kochkor MT Data

[8] The MT method relies on natural variations of Earth's magnetic field that induce electrical currents in the Earth [e.g., *Vozoff*, 1991]. Horizontal components of the vector electric field and all components of the vector magnetic field are recorded as time series at an MT site, and period-dependent, complex transfer functions between the magnetic and electric fields are calculated [e.g., *Larsen et al.*, 1996]. These transfer functions, called impedance tensors, from multiple sites along a profile are then inverted to yield a cross section of electrical conductivity which may be interpreted geologically.

[9] MT responses are usually sampled along a profile oriented perpendicular to structural strike and decomposed into two principal impedances oriented parallel (transverse electric (TE) mode) and perpendicular (transverse magnetic (TM) mode) to the strike for two-dimensional (2-D) structures [e.g., *Swift*, 1967]. Principal impedances can still be derived over 3-D structures, but their orientations are not necessarily related simply to the structural strike [e.g., *Park*, 1985; *Wannamaker et al.*, 1984]. Nonetheless, 2-D interpretation methods can often still be used for 3-D structures [*Wannamaker*, 1999]. A period-dependent, complex transfer function between the vertical and horizontal magnetic fields is also computed and usually presented as an induction vector. Induction vectors, based on the real components of the transfer function only, point typically toward 2-D conductors [*Schmucker*, 1970].

[10] The high-resolution MT profile following the Ukok River on the southeast side of the Kochkor basin (Figure 2) was selected because of road access across the range front and minimal anthropogenic electromagnetic noise. Near this section, two fault splays comprise the South Kochkor fault. A northern splay forms the contact between basement and basin strata, while the southern splay separates basement rocks and marks a topographic front. The northern splay of the South Kochkor fault provides a viable target for the MT method because it places resistive Ordovician (?) granite and granodiorite over conductive Neogene sandstone and Quaternary gravel [*Akademii nauk Kyrgyz Soviet Socialist Republic and Ministry of Geology*, 1980]. Although till and outwash sand and gravel cover much of the floor of the drainage in the hanging wall, outcrops of crystalline basement along the banks of the river indicate that these Quaternary deposits are thin and will likely not mask the underlying structure. The Akchop Hills fault, which juxtaposes Neogene and Quaternary sediments, provides a poor MT target, and the profile was thus terminated before it crossed this fault.

[11] The depth of penetration for MT fields is proportional to the square root of period; only short periods are needed in order to image shallow faults. The hypothesized subthrust sedimentary section beneath the Terskey Ala-Too range is expected to be in the upper 1–4 km, so only periods <100 s are used here. Fifty-four MT stations spaced 95 m apart formed a profile $\sim$5 km long (Figure 2) and perpendicular to the local strike of the South Kochkor fault. Time series were recorded simultaneously in blocks of five contiguous MT sites and at a remote reference site 7 km away with Electromagnetic Measurement, Incorporated's MT-24 system. Each block consisted of five collinear dipoles oriented parallel to the profile, one dipole oriented perpendicular to the profile, and one three-component magnetic field measurement. Time series were converted to tensor impedances and magnetic transfer functions using Larsen's robust processing program [*Larsen et al.*, 1996].

[12] MT impedance tensors are often distorted by shallow heterogeneities, and lack of correction may lead to incorrect orientations for the principal impedances [e.g., *Groom and Bailey*, 1989; *Chave and Smith*, 1994]. We use the Groom-Bailey decomposition [*Groom and Bailey*, 1989] to extract a 2-D regional azimuth from the data. This method represents the tensor in measurement coordinates as a combination of a 2-D regional tensor oriented along structural strike and distortion factors called twist and shear. A consistent 2-D geoelectrical strike of N80°E for periods <36 s resulted from the Groom-Bailey analysis. Because a consistent geoelectrical strike was found for the entire period range and this strike matches the geologic strike (Figure 2), we concluded that the distortion analysis correctly identified the proper geoelectrical strike. This conclusion is supported by the orientation of N60°W for the induction vectors at periods longer than 0.1 s (Figure 2), which should be oriented perpendicular to strike for 2-D conductors.

[13] The distortion analysis does not remove all of the effects of surficial heterogeneity, however [*Groom and Bailey*, 1989]. This residual, called a static shift, appears as a period-independent offset between the magnitudes of the two principal modes at the shortest periods. Static shifts determined by comparison of these magnitudes at the shortest periods (0.0025 s) between both modes and between adjacent sites ranged generally from 0.4–2.0, with some outliers as large as $\sim$6; these were removed from the data prior to inversion.

[14] The principal impedances are complex and are conventionally represented by a magnitude, called the apparent resistivity, and a phase. For multiple sites, cross sections of apparent resistivity (or phase) are plotted versus period (analogous to depth) and horizontal position (Figure 3). Pseudosections are often displayed with the comparisons to the simulated responses from a conductivity model derived from inversion; these comparisons will be discussed later in this section. The apparent resistivities for both principal impedances show resistive values to the south and more conductive values to the north (Figure 3). Both pseudosections show more resistive values at the shortest periods beneath sites 61–115 and more conductive values at intermediate periods. These patterns are consistent with a subthrust sedimentary section along the South Kochkor fault that extends as far south as site 51 (Figures 3 and 4). The

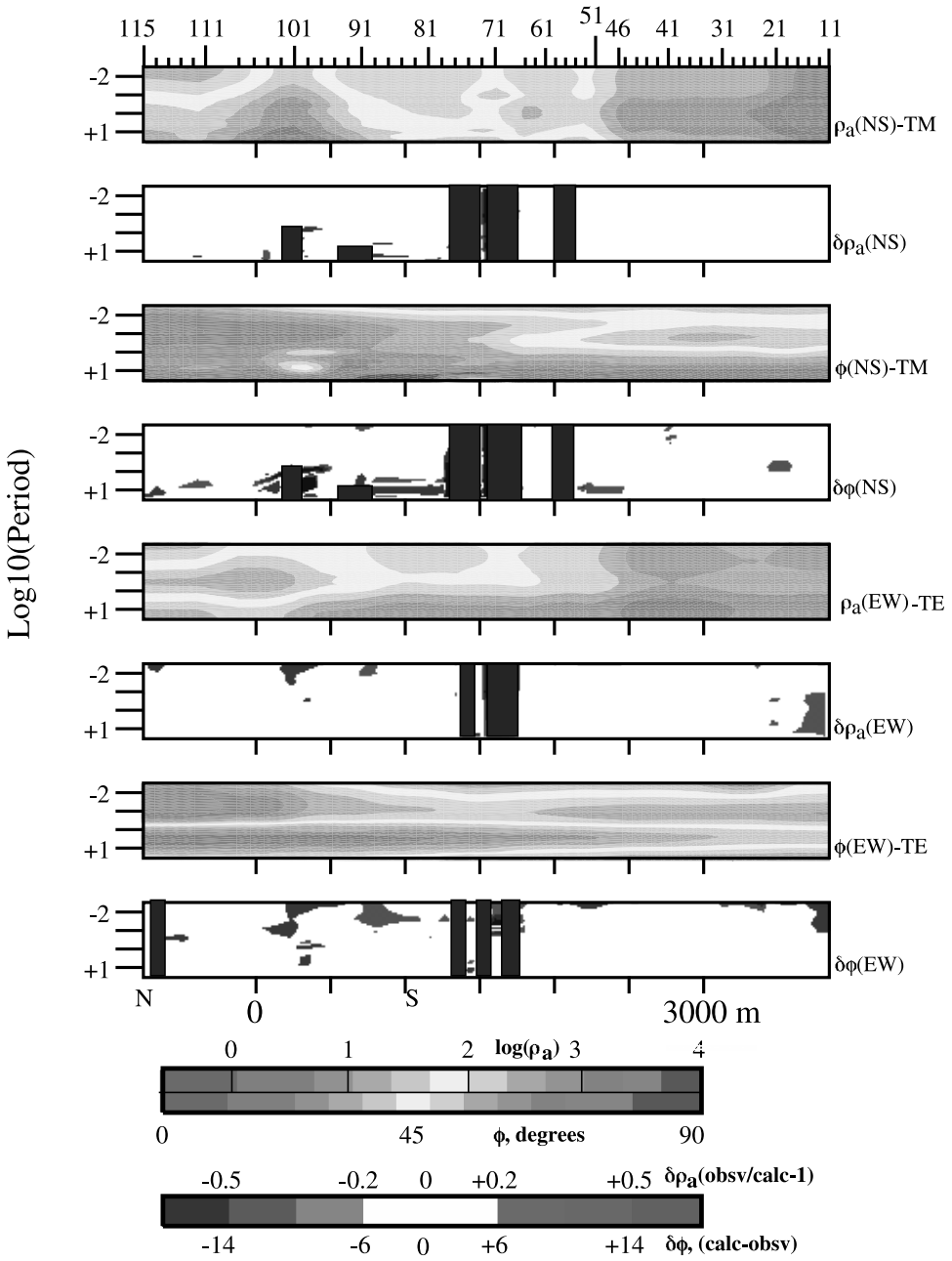

Figure 3. Pseudosections of MT data with difference pseudosections showing misfits between modeled responses and observed data. Pseudosections are plotted as horizontal position versus log10 (period). Upper scale bars are used for apparent resistivities (ρ_a) and phase (φ). Difference pseudosections are plotted as fractional differences between observed and calculated apparent resistivities and differences in phases. TM (NS) and TE (EW) modes are labeled. Site numbering is not sequential but uses the site numbers with which the data were recorded and archived. Data were recorded in blocks of five sites, which were numbered sequentially, but different blocks were incremented by an additive factor of 10. For example, sites 11–15 were recorded in a single block at the south end of the line. The second block placed site 21 (block 2, site 1) 95 m from site 15, thereby leaving a gap in site numbers from 16 to 20.

TM mode pseudosection also has low apparent resistivities beneath site 101, which are seen at all periods (ρ_a (NS) in Figure 3). While this feature may extend to depth, shallow conductors often screen deeper structure in the TM mode [*Wannamaker et al.*, 1984]. The relative uniformity of the TM phase beneath site 101 suggests that the good conductor is located only near the surface, however. Simple transformation of pseudosections into depth is unreliable because

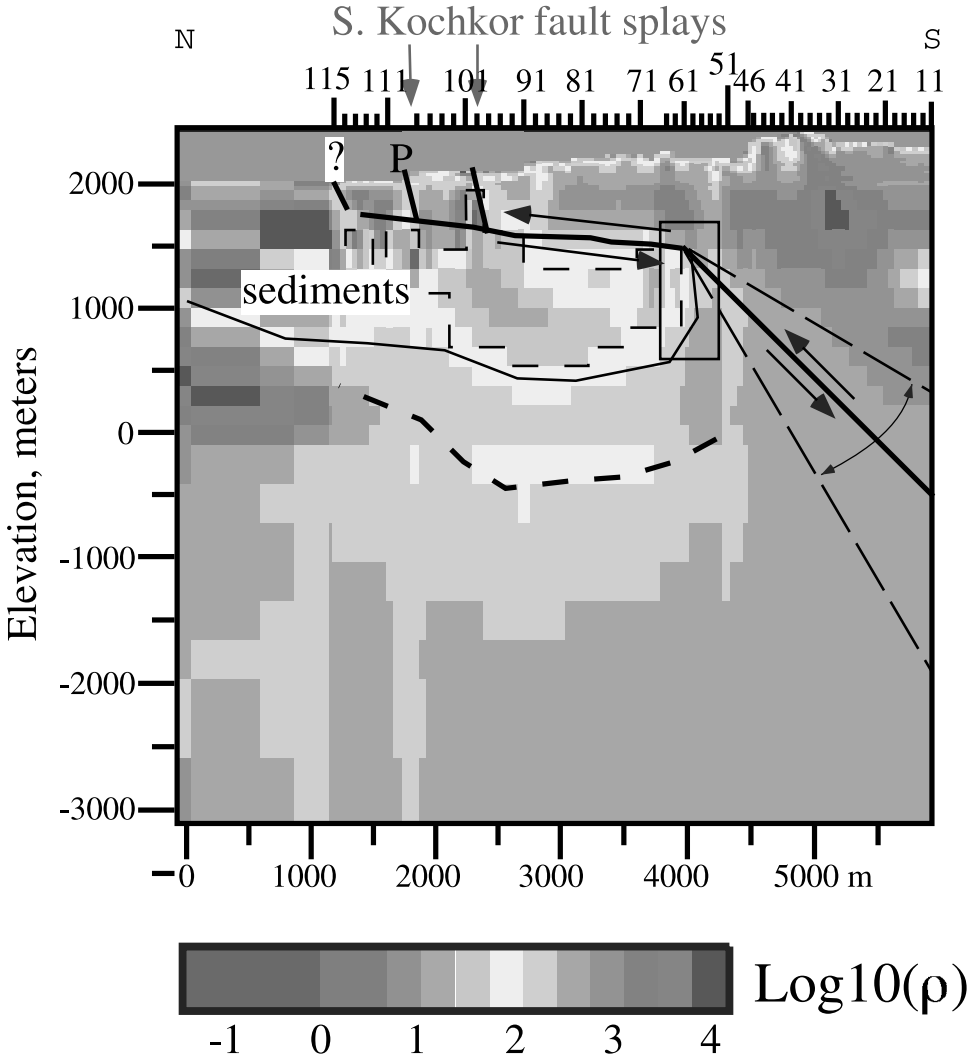

Figure 4. Preferred resistivity model for Kochkor MT profile. The active surface trace of the South Kochkor fault is shown in the gap south of site 111; the southern splay projects to site 95. The location of the pond near site 111 is also shown (P). The region outlined by the thin dashed line was tested for sensitivity to its resistivity. The region outlined by the rectangle beneath sites 53–71 shows the uncertainty in the placement of the southern edge of the conductive sediments. The bold dashed line shows the maximum depth to the base of the sediments. Faults and sediment-basement contact (thin solid line beneath "sediments") are based solely on resistivities.

the depth of penetration also depends on resistivity, and inversion must be used instead.

[15] Apparent resistivities and phases for both modes and the vertical magnetic transfer function were inverted using *Rodi and Mackie*'s [2001] 2-D regularized inversion algorithm that minimizes a combination of the x^2 measure of data misfit and the deviation from an a priori model. This choice of model penalty places great weight on the a priori model, and features in the starting model can be propagated as artifacts through the inversion. Our a priori model consisted of a simple, layered half-space with values determined from a 1-D inversion of the geometric mean of all 54 MT sites. The upper 7.5 km of the model was replaced with a uniform layer of 500 ohm m in order to prevent structural artifacts in this depth range. Only a subset of the model will be shown here; the actual model extends to the north and south for over 1000 km and to a depth of 600 km in order to achieve accurate simulations of the tensor impedances. The overall RMS error for our preferred model (Figure 4) after 223 iterations was 2.00, which meant that the simulated responses matched the observed ones to within twice our estimated errors for the data. Estimated errors were based on the larger of the calculated errors from the data analysis or the scatter of estimates between adjacent periods (5% for the TM amplitude, TM phase, and TE phase and 15% for the TE amplitude and Hz transfer function). The larger error for the TE amplitudes was chosen because these can be affected by the 3-D structure off the profile [*Wannamaker*, 1999].

[16] Plotted with the pseudosections (Figure 3) are misfits between the simulated responses from our preferred model and the observed data. The TM mode apparent resistivities are generally fit to within 4%, and both phases are fit to within 5°. No systematic patterns of misfit (higher misfits at certain periods or alternatively at certain sites) are seen. The TE mode apparent resistivity is consistently underestimated to the north and overestimated to the south (ρ_a (EW) in Figure 3), but larger misfits are expected because this parameter was downweighted in the inversion.

4. Resistivity Model

[17] The preferred resistivity model resulting from 2-D inversion of the MT data shows a clear conductive region at elevations above sea level (asl) of 400–1800 m, with resistivities <100 ohm m beneath a ~500-m-thick layer of rocks with resistivities >100–300 ohm m (Figure 4). These resistive rocks are also found below the southern 2 km of the profile and beneath the conductive region at elevations below ~400 m. We infer that resistivities <100 ohm m are due to water-saturated sediments and/or fluid migration along fault zones, whereas values >300 ohm m are indicative of crystalline basement rocks. Resistivity values between 100 and 300 ohm m cannot be clearly identified as either sediment or basement and are therefore not assigned to a specific rock type.

[18] The overlying resistive rocks near the surface extending from site 115 in the north to site 51 in the south are not continuous but rather are broken up with conductive zones extending to the surface (Figure 4). The prominent discontinuities at site 95 and the gap between sites 105 and 111 (Figure 4) coincide with strands of the South Kochkor fault (Figure 2). The conductive zone beneath site 85 may also be an unmapped fault, but no geological corroboration exists. We made no measurements in the gap between sites 105 and 111 because a pond had formed from a leaking irrigation canal. This canal is sited at the base of a fault scarp marking the fault, and we infer that the zone of enhanced conductivity here is due to fluid leakage down the fault zone.

[19] The resistive block beneath sites 111–115 at elevations above 1400 m asl lies clearly to the north of the South Kochkor fault (Figures 2 and 4) in the footwall. The resistivity of this block is constrained well by the data, indicating that basement rocks extend at least as far north as site 115. The contact between the northern end of this basement and the Cenozoic sediments is either a fault or an unconformity buried beneath the Quaternary deposits at the surface.

[20] One confusing aspect of our preferred model is the presence of both resistive (>300 ohm m) and extremely conductive rocks (<1 ohm m) at elevations above 900 m asl and north of our profile (Figure 4). Our geologic mapping suggests that these rocks should be Neogene sediments (Figure 2). While low resistivities are expected for the sediments, how can we explain the more resistive rocks? The higher resistivities appear for two reasons. First, in the absence of any sensitivity to a particular cell in the model the resistivity will presumably remain unchanged from the value in the a priori model (500 ohm m). Values above 1400 m asl near 500 ohm m are likely the result of insensitivity to these regions. The high resistivity (>10,000 ohm m) just north of the profile is a consequence of low sensitivity. Because MT impedances and vertical magnetic field transfer functions are much more sensitive to conductive regions than to resistive ones, the inversion can place large increases in resistivity in regions with low sensitivity. This positive feedback (increasing the resistivity lowers the sensitivity further, thereby permitting larger increases) results in the appearance of resistive artifacts in regions with no data. The most important property of the region to the north of the profile is its cross-sectional conductance. The influence of the low resistivities dominates over that of the high values, and the region north of the profile has high cross-sectional conductance. This high cross-sectional conductance appears in the model because the MT fields have some sensitivity to the thick conductive sedimentary section in the Kochkor basin to the north. The details of that conductivity distribution to the north cannot be resolved because of lack of data, however.

[21] Superimposed on the MT model is a simple structural interpretation based solely on comparison of resistivities to the surface geology (Figure 4). Two splays of the South Kochkor fault are shown crossing the section at the locations of shallow, vertical conductors. We infer that the subthrust sediments extend as far south as site 61, based on low resistivities to the north and the high conductivity gradient at depths of 900–1400 m asl beneath that site (Figure 4). Rocks are much more resistive throughout the section south of site 51, indicating more competent basement rocks and the absence of sediments in this region. The thin solid line (Figure 4) outlines our preferred sedimentary section and is based on the distribution of resistivities <100 ohm m. We discuss the uncertainties in the thickness and resistivity of the sediments in section 5. The thrust fault, dipping 45° southward and based on the depth extent of resistivities >300 ohm m, is diagrammatic. This fault is placed where it separates the shallow, resistive block in the hanging wall at elevations of 0–1400 m asl from the background resistivity of the a priori model of 500 ohm m in the footwall block. We discuss its dip and location in section 5.

5. Confidence Limits for Resistivity Model

[22] Our resistivity model results from the inversion of the MT impedances and transfer functions, which provides fewer constraints than there are model blocks and could contain resistivity artifacts [e.g., *de Groot-Hedlin and Constable*, 1990]. Bounds on the resistivities and geometries of geologically significant portions of the preferred model (Table 1) were established with over 60 additional inversions; details of this analysis are provided in Appendix A. On the basis of misfits at individual sites (Figure 5) we conclude that an average resistivity of 10 ohm m for subthrust sediments is preferred, but a value as high as 20 ohm m is still acceptable. However, an average value of 30 ohm m does not fit the data well. The subthrust

Table 1. Summary of Sensitivity Tests

Parameter Tested	Bounds
Resistivity of subthrust sediments, ohm m	10–20
Thickness of subthrust sediments, m	1000–2000
Lateral position of thrust, m	350 N to 100 S
Dip of fault zone, deg	30–60

sedimentary section is also contiguous with the conductor to the north, which we infer to be due to saturated sediments in the Kochkor basin.

[23] The maximum depth to which the sediments could extend beneath the level indicated in the preferred model lies at an elevation −600 to +400 m asl (bold dashed line in Figure 4) and is based on the range of average resistivity of the sediments (see Appendix A). Combined with our preferred model, this means that the sedimentary section could be as thin as 1000 m and as thick as 2000 m. Related to this test of the cross-sectional area of sediment in the subthrust section is the southernmost extent of the edge of this section (solid box between sites 53 and 71 in Figure 4).

[24] The north and south edges of the outlined box between sites 53 and 71 (Figure 4) show how far the vertical contact between the basement and sediment can be moved before misfits at individual sites exceed the errors at those sites; the upper and lower edges were chosen based on the average depth range of the conductive sediments in the preferred model (Figure 4). The southern end of the sedimentary section can be moved no more than 350 m south or 100 m north of its preferred location beneath site 61 (Table 1). While the sediments do not extend as far south as the thrust ramp in the preferred model (Figure 4), the southern edge of the box extends to the crustal ramp, and sediments could therefore be in contact with this ramp.

[25] Finally, the thrust ramp beneath sites 11–51 (Figure 4) is constrained to dip between 30° and 60°S (Table 1). We place this thrust where it separates the shallow, resistive block in the hanging wall at elevations of 0–1400 m asl from the a priori resistivity of 500 ohm m in the footwall. While the fault bend beneath site 61 could be as much as 500 m north, tests of the dip of the ramp were run with only the fault bend shown (Figure 4). Modeling (see Appendix A) shows that this fault can have a dip no shallower than 30° and no steeper than 60°. While this range of dips is large for structural control, it is remarkable that the MT method is able to provide such constraints at all.

6. Discussion

[26] A geologic cross section (Figure 6), based on the MT model in Figure 4, provides a viable solution for the deformation beneath the southern Kochkor basin and links the crustal ramp, the gently dipping fault beneath sites 61–115, and the Akchop Hills thrust. We infer that the gently dipping fault between sites 61–115 (Figure 4) is a décollement underlying the Ukok River. The presence of a shallow décollement is consistent with the surface geology (Figure 2); the narrow panel of Neogene strata exposed in the hanging wall of the Akchop Hills fault east and west of the Ukok River indicates that the dip of the Akchop Hills thrust decreases to a gentle dip at a shallow depth. The interpretation that basement rock overlies subthrust Tertiary sediment along the décollement beneath the range front, and that a moderately dipping thrust ramp underlies the Terskey Ala-Too range, provides a reasonable geometric solution to reconcile current shortening on the Akchop Hills fault with growing structural relief across the range-basin margin.

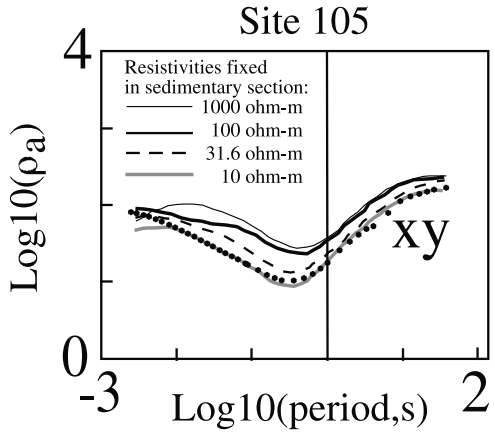

Figure 5. Example of sensitivity testing at site 105. Data points with errors are shown by circles, while model responses are shown by different line patterns. Note how a value of 10 ohm m fits the data best. Other results (not shown here) provide equivalent fits with a resistivity of 20 ohm m.

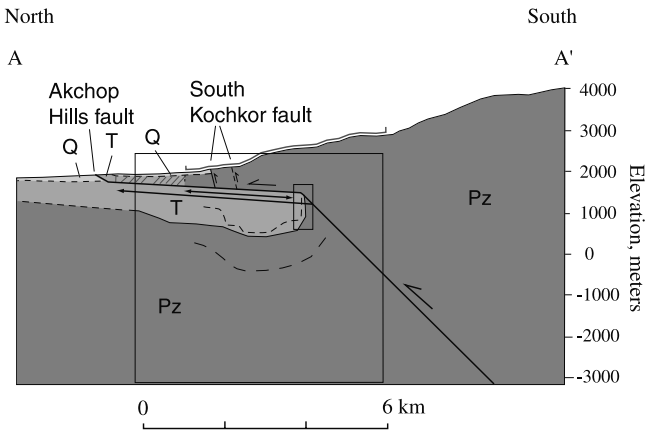

Figure 6. Geologic cross section based on mapped structure (Figure 2) and the resistivity model (Figure 4). The solid box outlined in the center of the cross section shows the location of the resistivity model in Figure 4. The shaded line above the topography shows the extent of MT soundings. The Paleozoic basement rocks in the hanging wall of the décollement extend north to at least the end of the MT profile line but must end south of the Akchop Hills fault. The amount of underthrusting of the sedimentary section beneath the range front is a minimum of ∼3 km. Structural relief on the top of Paleozoic basement across the range front is at least 3.7 km.

[27] The MT model and the geologic interpretation diverge, however, with the shallow, highly resistive body north of the South Kochkor fault between sites 111 and 115 (Figure 4). On the basis of air photo analysis and previous geologic mapping along the Djuanarik River the footwall block of the South Kochkor fault was expected to consist of Neogene and Quaternary basin strata (Figure 2). The MT model clearly predicts Paleozoic basement rocks to the north of the mapped South Kochkor fault, extending to at least the north end of the MT profile line. Because the air photo interpretation does not preclude basement in the fault footwall, we interpret basement to extend northward to at least the end of the MT profile line. In this scenario, Quaternary debris flow and alluvial fans and Ukok River alluvium conceal basement rock north of the South Kochkor fault. The basement rock can extend no farther north than the Neogene strata exposed in the hanging wall of the Akchop Hills fault, however (Figures 2 and 6). The buried contact between Paleozoic basement and Neogene strata in the hanging wall block of the décollement could be either a fault or a depositional contact.

[28] A simple interpretation of the cross section suggests a two-phase evolution of the basin margin. The vertical contact of the southern margin of the sediments indicates synclinal folding of the footwall block, likely related to an early period of fault propagation folding. Footwall folding in basement during fault propagation folding has been observed in some Laramide structures [*Schmidt et al.*, 1993; *Narr and Suppe*, 1994]. At least 1–2 km of syntectonic strata were deposited in the synclinal depression during this initial phase.

[29] A second phase of deformation involved faults breaking through the basement fault propagation fold; these include the South Kochkor fault strands and the Akchop Hills décollement. The relative timing of the breakthrough faults cannot be resolved, so they are grouped in this second phase. Because the décollement is shallow and overlies 1–2 km of strata, this fault must have formed relatively late in the history of deformation here. The higher rate of late Quaternary slip on the Akchop Hills fault [*Thompson et al.*, 2002] simply implies that most slip generated along the crustal ramp is translated to the surface along the extent of the décollement and relatively little shortening is absorbed by the high-angle splays of the South Kochkor fault.

[30] At the southern margin of the Kochkor basin, at least 2.5 km of displacement on the décollement has occurred, offsetting the basement-sediment contact in the hanging wall from the footwall cutoff near the deeper crustal ramp. Movement of material over the crustal ramp-to-décollement fault bend requires anticlinal folding of granitic basement rocks [*Narr and Suppe*, 1994]. The folding of crystalline rocks by brittle deformation mechanisms in the upper ~1 km of crust is perhaps surprising [cf. *Schmidt et al.*, 1993].

[31] Our first-order results from the southern margin of Kochkor basin include (1) strata thrust beneath the basin margin along a low-angle décollement and (2) an offset of range front structures at the surface from the deeper crustal ramp and provide a kinematic explanation whereby the more active fault lies within the basin interior and not at the range-basin margin. These results support cross-section solutions proposed by several other workers in areas of thick-skinned mountain building, including the Japanese Alps [*Ikeda*, 1983], the Transverse Ranges of southern California [*Ikeda*, 1983], the Po basin in Italy [*Benedetti et al.*, 2000], and elsewhere in the Tien Shan [*Avouac et al.*, 1993; *Brown et al.*, 1998; *Burchfiel et al.*, 1999; *Bullen et al.*, 2001; *Thompson et al.*, 2002]. Clearly, compressive structures within foreland basins can be underlain by thrust faults that involve basement directly [e.g., *Stone*, 1993], but our MT model from the Ukok River shows that the active fault within the basin interior connects at a shallow depth with the same crustal ramp that vertically offsets the range from the adjacent basin.

[32] The thrust fault geometry interpreted at the southern Kochkor basin has basic implications for earthquake hazard and active tectonics studies. First, the crustal ramp that accumulates and releases elastic strain energy during earthquakes may be offset by several kilometers from the surface fault traces. This affects both predictions of shaking hazards during earthquakes [*Yeats et al.*, 1997] and the prediction of zones of elastic strain accumulation over locked portions of faults [*Meade and Hager*, 2001]. Second, surface faults in the basin interior and at the range front should not be considered separate earthquake sources if they have a shared crustal ramp through seismogenic depths.

7. Implications for Shortening at Kochkor Basin and Tien Shan Tectonics

[33] The MT data provide constraints on the subsurface geometry that allow rough calculations for the amount and partitioning of shortening across the active southern margin of the Kochkor basin. The structural relief on the top of basement, a Paleozoic-Cenozoic unconformity [*Makarov*, 1977], and the dip of the underlying crustal ramp provide a simple measure of total shortening across the southern margin. We infer that peak elevations and ridge crests approximate the original extent of the unconformity [*Makarov*, 1977; *Sadybakasov*, 1972; *Abdrakhmatov et al.*, 2001]. The peak elevations of the Terskey Ala-Too range south of the Ukok River are ~4100 m; the depth to the top of basement imaged by MT is −600–400 m asl (Figure 6). The structural relief is therefore 3700–4700 m; in our uncertainties we permit a maximum of 300 m of peak erosion to get a range of 3700–5000 m structural relief. The dip of the crustal ramp is constrained by the MT data to be 45°±15° (Table 1). Assuming 2-D, rigid block deformation, crustal shortening equals structural relief divided by the tangent of the fault dip. Crustal shortening equals 3.9 + 3.6/−1.5 km at a 95% confidence if we allow a uniform probability distribution for structural relief and a normal probability distribution for the dip of the crustal ramp. Part or all of this 2.4- to7.5-km shortening is reflected in the offset along the shallow décollement.

[34] The total displacement along the décollement depends on the northernmost extent of basement in the hanging wall and southernmost extent of sediments in the

footwall. Assuming that basement extends at least as far north as site 115 (Figure 4) and the sediments extend no farther south than site 71, the minimum displacement is 2.5 km. The maximum value is 4.8 km, assuming that basement extends as far north as the Neogene strata exposed in the hanging wall of the Akchop Hills fault and that the subthrust sediments extend as far south as site 53 (Figures 4 and 6). This offset of 2.5–4.8 km is the portion of total shortening accommodated by the décollement. The minimum amount of underthrusting (2.5 km) exceeds the minimum amount of total shortening estimated above (2.4 km), which is impossible because the décollement initiated after some of the structural relief developed. We therefore revise our total shortening estimate to a range of >2.5–7.5 km.

[35] Average shortening rates estimated from our cross section differ from late Quaternary rates, indicating that shortening has accelerated in the past several million years. The age at the base of the Tertiary section in the Kochkor basin has been estimated to be ~12–13 Ma, based on a magnetic stratigraphy measured near the Djuanarik River [*Abdrakhmatov et al.*, 2001]. The total shortening divided by the basin age gives a long-term shortening rate of >0.2–0.6 mm yr^{-1}. This rate is an order of magnitude less than the ~3 mm yr^{-1} rate of shortening in the late Quaternary [*Thompson et al.*, 2002]. Our results are consistent with studies at the northern margin of the Tien Shan [*Bullen et al.*, 2001] and other intermontane basins in the central Tien Shan [*Abdrakhmatov et al.*, 2001], showing that rates of crustal shortening increased in the past several million years, much later than the initial period of basin formation and sediment accumulation ~11–14 Ma [*Bullen et al.*, 2001; *Sobel and Dumitru*, 1997; *Abdrakhmatov et al.*, 2001].

[36] The amount of displacement along the décollement and its relatively late development also indicate accelerating shortening rates. The décollement accounts for a minimum of 33% and a maximum of 100% of the total shortening of >2.5–7.5 km. If offset along the décollement occurred solely at the late Quaternary rate of ~3 mm yr^{-1}, then this fault initiated ~0.8–1.6 Ma. At least one third of the total shortening across the Kochkor basin may have developed only during the most recent ~10% of the Kochkor basin's history.

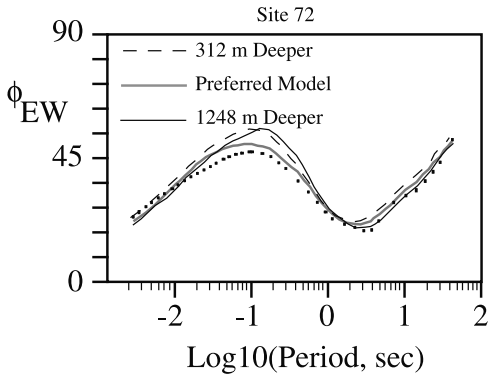

Figure A1. Sensitivity tests for maximum depth to base of sediments. Note how increasing the thickness of the 10-ohm m layer beneath the sediment affects the phase misfit centered at a period of 0.1 s. Misfits were apparent even with a minimum increase of 312 m.

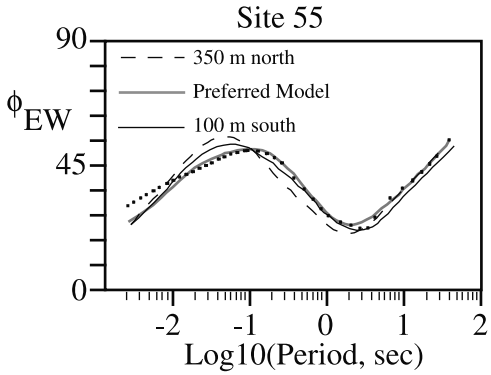

Figure A2. Sensitivity tests for southernmost edge of subthrust sediments. Note how shifting the edge either north or south affects the phase data from periods of 0.001–3 s, with a pronounced misfit at a period of 0.05 s.

8. Conclusions

[37] A high-resolution MT profile yields a resistivity model with a clear image of subthrust sediments at the margin of an intermontane basin in the central Tien Shan. A geologic cross section constrained by the resistivity model shows a shallow, gently dipping décollement connecting the steeper crustal ramp to an active thrust within synorogenic strata. On the basis of this connection we infer that the range-bounding fault and the intrabasin thrust should be treated as a single structure in any estimates of geodetic strain or earthquake hazard. Total shortening of >2.5–7.5 km on this structure is estimated from the geologic section and uncertainties in the depth to basement and dip of the crustal ramp, both constrained by the MT data. Displacement along the shallow décollement alone accounts for at least one third, and conceivably all, of the total convergence. The décollement developed late in the history of the basin and therefore experienced shortening rates that were faster than the average rate since basin inception. Combined with estimates of ages for the sediments, our section confirms increasing shortening rates since basin inception.

Appendix A

[38] Sensitivity tests consist of perturbing structural features of the preferred model (Figure 4), fixing them in an inversion, and allowing the inversion to search for an alternate model that fits the data equally well. The first tests assessed the existence of the subthrust sedimentary section and established bounds on the resistivities of the sediments (Table 1). Resistivity values in the subthrust section (outlined by the dashed line in Figure 4) were fixed at 0.5-decade intervals from 3.16–3160 ohm m in a series of inversions. None of these test models fit the data as well as the preferred model because the latter had variable resistivity values within the sediments; the test models had a single, fixed value. Nonetheless, the overall RMS error for the misfit between the

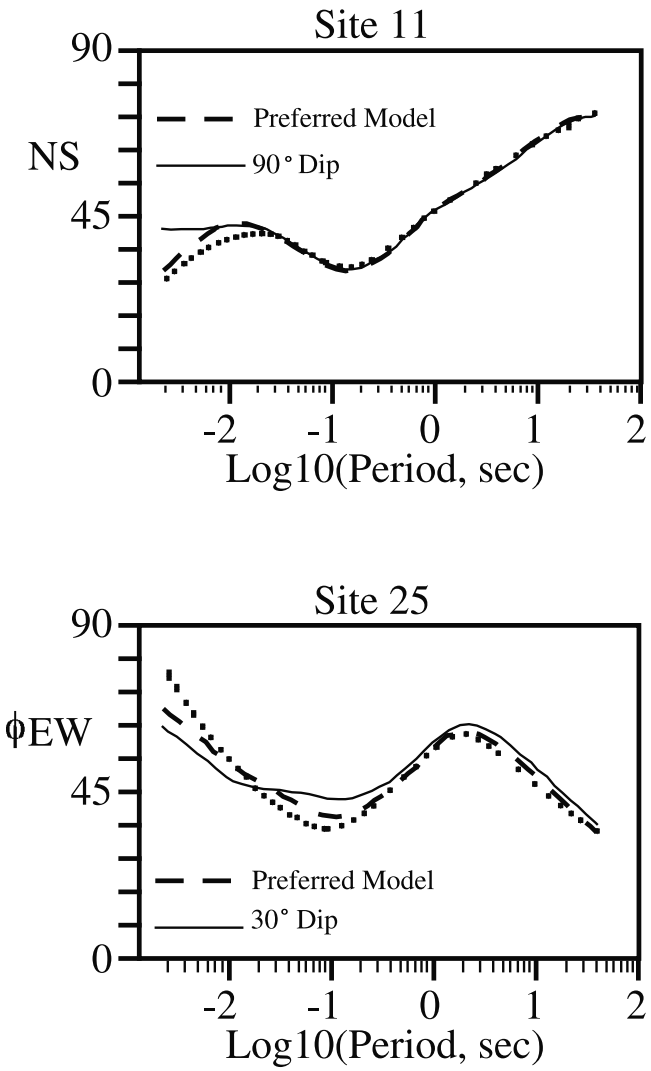

Figure A3. Sensitivity tests for fault dip. Two different sites are shown because the fault dip affected sites differently. Note that most of the misfit occurs at periods <0.02 s.

data and the responses from the test models did not vary dramatically (2.0–3.3). Individual sites showed misfits that exceeded the errors for the data, however (Figure 5). The maximum depth to the base of the sediments was determined by placing a 10-ohm m layer beneath the sediments in Figure 4 and gradually thickening it. Thickening this layer by as little as 312 m affects the TE (EW) phase at site 72 appreciably (Figure A1). Increasing the thickness dramatically by 1248 m produced no additional changes in the misfit. We therefore conclude that the sediments could be as thin as 1000 m (i.e., no change in thickness from the preferred model in Figure 4). We show a maximum thickness of ~2000 m in Figure 4 because of the uncertainty in the resistivity of the sediments. Our depth tests were run with 10 ohm m, but values of 20 ohm m are plausible for the sediments. In the limit of very thin layers the MT responses to first order are sensitive to cross-sectional conductance ($\Delta Z \Delta X/\rho$). To estimate the maximum bound on the sediment thickness, we doubled the preferred value of 1000 m to account for the possibility that the sediments could have resistivities as large as 20 ohm m. This is likely an overestimate of the maximum thickness and therefore represents a conservative value.

[39] The north-south extent of the subthrust section is constrained by the TE (EW) phase (Figure A2). Misfits are most noticeable compared with the preferred model in the period range of 0.01–0.1 s, although they are also seen over the entire range of periods longer than 0.01 s (Figure A2). The tests were performed by adding conductive material to the south or adding resistive material to the north. The larger uncertainty to the north (350 m) results from the inversion simply decreasing the resistivity of the sediments to the north in order to compensate for the loss of conductive material in the fixed region. Such compensation is much more difficult when additional conductors are added to the section, as in the case of extending the sediments to the south.

[40] The most unexpected result from the sensitivity tests was that the MT data could be used to constrain the dip of a fault offsetting Paleozoic basement (Figure 4). Forward modeling (not shown here) with a 50:1 resistivity contrast between sediments and basement showed that responses for dips <30° were indistinguishable from those calculated for horizontal layers of appropriate thickness. Forward modeling also showed that contacts with dips >60° had responses similar to those from vertical contacts. Two inversions were run with the fault dip in Figure 4 constrained to be 30°and 90° (Figure A3), with resistivity contrasts of 20:1–50:1. In both cases the misfits are appreciable in the phase data. Different sites are shown in Figure A3 because we are showing the sites with the maximum misfits; in most cases, the overall RMS error for the entire profile was not altered substantially from that of the best fitting model. Misfits between the data and preferred model at sites 11 and 25 for periods <0.01 s are seen, but the test models show an even greater deviation from the data. We therefore conclude that bounds on the fault dip of 30° and 60° are justifiable.

[41] **Acknowledgments.** We would like to thank our Russian colleagues from IVTRAN in the Kyrgyz Republic for their participation in the MT data acquisition and for their logistical support. We thank K. Abdrakhmatov, J. Unruh, and R. Yeats for helpful discussions and P. Wannamaker, R. Weldon, and associate editor C. Jones for helpful (if painful!) reviews. This project was funded by grant EAR9613760 to UC Riverside from the National Science Foundation Continental Dynamics program. The MT24 system was borrowed from the EMSOC Consortium, which was funded by grant EAR9616986 to UC Riverside from the National Science Foundation Instrumentation and Facilities program.

References

Abdrakhmatov, K., R. Weldon, S. Thompson, D. Burbank, C. Rubin, M. M. Miller, and P. Molnar, Origin, direction, and rate of modern compression of the central Tien Shan (Kyrgyzstan) (in Russian), *Geol. Geofiz.*, *42*, 1585–1609, 2001.

Akademii nauk Kyrgyz Soviet Socialist Republic and Ministry of Geology, Geological Map of the Kyrgyz SSR, scale 1:500,000, USSR, 1980.

Avouac, J. P., P. Tapponnier, M. Bai, H. You, and G. Wang, Active thrusting and folding along the northern Tien Shan and late Cenozoic rotation of the Tarim relative to Dzungaria and Kazakhstan, *J. Geophys. Res.*, *98*, 6755–6804, 1993.

Beauchamp, W., R. W. Allmendinger, M. Barazangi, A. Demnati, M. El Alji, and M. Dahmani, Inversion

tectonics and the evolution of the High Atlas Mountains, Morocco, based on a geological-geophysical transect, *Tectonics*, *18*, 163–184, 1999.

Bedrosian, P. A., M. J. Unsworth, and F. Wang, Structure of the Altyn Tagh Fault and Daxue Shan from magnetotelluric surveys: Implications for faulting associated with the rise of the Tibetan Plateau, *Tectonics*, *20*, 474–486, 2001.

Benedetti, L., P. Tapponnier, G. C. P. King, B. Meyer, and I. Manighetti, Growth folding and active thrusting in the Montello region, Veneto, northern Italy, *J. Geophys. Res.*, *105*, 739–766, 2000.

Berg, R. R., Mountain flank thrusting in the Rocky Mountain foreland, Wyoming and Colorado, *Am. Assoc. Pet. Geol. Bull.*, *46*, 2019–2032, 1962.

Brown, E. T., D. L. Bourles, B. C. Burchfiel, Q. Deng, J. Li, P. Molnar, G. M. Raisbeck, and F. Yiou, Estimation of slip rates in the southern Tien Shan using cosmic ray exposure dates of abandoned alluvial fans, *Geol. Soc. Am. Bull.*, *110*, 377–386, 1998.

Bullen, M. E., D. W. Burbank, J. I. Garver, and K. Y. Abdrakhmatov, Late Cenozoic tectonic evolution of the northwestern Tien Shan: New age estimates for the initiation of mountain building, *Geol. Soc. Am. Bull.*, *113*, 1544–1559, 2001.

Burchfiel, B. C., E. T. Brown, D. Qidong, F. Xianyue, L. Jun, P. Molnar, S. Jianbang, W. Zhangming, and Y. Huichuan, Crustal shortening on the margins of the Tien Shan, Xinjiang, China, *Int. Geol. Rev.*, *41*, 665–700, 1999.

Chave, A. D., and J. T. Smith, On electric and magnetic galvanic distortion tensor decompositions, *J. Geophys. Res.*, *99*, 4669–4682, 1994.

de Groot-Hedlin, C., and S. Constable, Occam's inversion to generate smooth two-dimensional models from magnetotelluric data, *Geophysics*, *55*, 1613–1624, 1990.

Ghose, S., M. W. Hamburger, and C. J. Ammon, Source parameters of moderate-sized earthquakes in the Tien Shan, central Asia, from regional moment tensor inversion, *Geophys. Res. Lett.*, *25*, 3181–3184, 1998.

Global Land One-Kilometer Base Elevation Task Team et al., The Global Land One-Kilometer Base Elevation (GLOBE) digital elevation model, version 1.0, http://www.ngdc.noaa.gov/seg/topo/globe.shtml, Natl. Geophys. Data Cent., Boulder, Colo., 1999.

Gries, R. R., Oil and gas prospecting beneath Precambrian of foreland thrust plates in Rocky Mountains, *AAPG Bull.*, *67*, 1–28, 1983.

Groom, R. W., and R. C. Bailey, Decomposition of magnetotelluric impedance tensors in the presence of local three-dimensional galvanic distortion, *J. Geophys. Res.*, *94*, 1913–1925, 1989.

Ikeda, Y., Thrust-front migration and its mechanism: Evolution of intraplate thrust fault system, *Bull. Dep. Geogr. Univ. Tokyo*, *15*, 125–159, 1983.

Jordan, T. E., and R. W. Allmendinger, The Sierras Pampeanas of Argentina: A modern analogue of Rocky Mountain foreland deformation, *Am. J. Sci.*, *286*, 737–764, 1986.

Larsen, J. C., R. L. Mackie, A. Manzella, A. Fiordelisi, and S. Rieven, Robust smooth magnetotelluric transfer functions, *Geophys. J. Int.*, *124*, 801–819, 1996.

Makarov, V. I., *Neotectonic Structures of the Central Tien Shan* (in Russian), 171 pp., Akad. Sci., Moscow, 1977.

Meade, B. J., and B. H. Hager, The current distribution of deformation in the western Tien Shan from block models constrained by geodetic data (in Russian), *Geol. Geofiz.*, *42*, 1622–1633, 2001.

Mellors, R. J., F. L. Vernon, G. L. Pavlis, G. A. Abers, M. W. Hamburger, S. Ghose, and B. Iilasov, The *Ms* = 7.3 1992 Suusamyr, Kyrgyzstan, earthquake: 1. Constraints on fault geometry and source parameters based on aftershocks and body-wave modeling, *Bull. Seismol. Soc. Am.*, *87*, 11–22, 1997.

Narr, W., and J. Suppe, Kinematics of basement-involved compressive structures, *Am. J. Sci.*, *294*, 802–860, 1994.

Park, S. K., Distortion of magnetotelluric sounding curves by three-dimensional structures, *Geophysics*, *50*, 785–797, 1985.

Rodgers, D. A., and W. D. Rizer, Deformation and secondary faulting near the leading edge of a thrust fault, in *Thrust and Nappe Tectonics*, edited by K. R. McClay and N. J. Price, pp. 65–77, Blackwell Sci., Malden, Mass., 1981.

Rodi, W. L., and R. L. Mackie, Nonlinear conjugate gradients algorithm for 2-D magnetotelluric inversion, *Geophysics*, *66*, 174–187, 2001.

Sadybakasov, I., *Neotectonics of the Central Tien Shan* (in Russian), 117 pp., Ilim, Frunze, Russia, 1972.

Schmidt, C. J., R. B. Chase, and E. A. Erslev (Eds.), *Laramide Basement Deformation in the Rocky Mountain Foreland of the Western United States*, *Spec. Pap.Geol. Soc. Am.*, *280*, 358 pp., 1993.

Schmucker, U., Anomalies of geomagnetic variations in the southwestern United States, Ph.D. dissertation, Univ. of Calif., San Diego, Calif., 1970.

Smithson, S. B., J. Brewer, S. Kaufman, J. Oliver, and C. Hurich, Nature of the Wind River thrust, Wyoming, from COCORP deep-reflection data and from gravity data, *Geology*, *6*, 648–652, 1978.

Snyder, D. B., V. A. Ramos, and R. W. Allmendinger, Thick-skinned deformation observed on deep seismic reflection profiles in western Argentina, *Tectonics*, *9*, 773–788, 1990.

Sobel, E. R., and T. A. Dumitru, Thrusting and exhumation around the margins of the western Tarim Basin during the India-Asia collision, *J. Geophys. Res.*, *102*, 5043–5063, 1997.

Stone, D. S., Basement-involved thrust-generated folds as seismically imaged in the subsurface of the central Rocky Mountain foreland, in *Laramide Basement Deformation in the Rocky Mountain Foreland of the Western United States*, edited by C. J. Schmidt, R. B. Chase, and E. A. Erslev, *Spec. Pap. Geol. Soc. Am.*, *280*, 271–318, 1993.

Swift, C. M., Jr., A magnetotelluric investigation of an electrical conductivity anomaly in the southwestern United States, Ph.D. dissertation, Mass. Inst. of Technol., Cambridge, 1967.

Tapponnier, P., and P. Molnar, Active faulting and Cenozoic tectonics of the Tien Shan, Mongolia, and Baykal regions, *J. Geophys. Res.*, *84*, 3425–3459, 1979.

Thompson, S. C., R. J. Weldon, C. M. Rubin, K. Abdrakhmatov, P. Molnar, and G. W. Berger, Late Quaternary slip rates across the central Tien Shan, Kyrgyzstan, central Asia, *J. Geophys. Res.*, *107*(B9), 2203, doi:10.1029/2001JB000596, 2002.

Unsworth, M. J., P. E. Malin, G. D. Egbert, and J. R. Booker, Internal structure of the San Andreas Fault at Parkfield, California, *Geology*, *25*, 359–362, 1997.

Vozoff, K., The magnetotelluric method, in *Electromagnetic Methods in Applied Geophysics*, edited by M. N. Nabighian, pp. 641–711, Soc. of Explor. Geophys., Tulsa, Okla., 1991.

Wannamaker, P. E., Affordable magnetotellurics: Interpretation in natural environments, in *Three-Dimensional Electromagnetics*, *Geophys. Dev. Ser.*, vol. 7, edited by M. Oristaglio and B. Spies, pp. 349–374, Soc. of Explor. Geophys., Tulsa, Okla., 1999.

Wannamaker, P. E., G. W. Hohmann, and S. H. Ward, Magnetotelluric responses of three-dimensional bodies in layered earths, *Geophysics*, *49*, 1517–1533, 1984.

Yeats, R. S., K. Sieh, and C. R. Allen, *The Geology of Earthquakes*, 568 pp., Oxford Univ. Press, New York, 1997.

V. Batalev and A. Rybin, Institute for High Temperatures of the Russian Academy of Sciences Scientific Station, Bishkek 720049, Kyrgyz Republic. (rybin@tiger.gdirc.ru)

R. Bielinski and S. K. Park, Institute of Geophysics and Planetary Physics, University of California, 1432 Geology, Riverside, CA 92521-0412, USA. (rbiel@ucrmt.ucr.edu; magneto@ucrmt.ucr.edu)

S. C. Thompson, Department of Geological Sciences, 1272 University of Oregon, Eugene, OR 97403-1272, USA. (stevet@uwashington.edu)